Frontiers of Information Technology & Electronic Engineering
www.jzus.zju.edu.cn; engineering.cae.cn; www.springerlink.com
ISSN 2095-9184 (print); ISSN 2095-9230 (online)
E-mail: jzus@zju.edu.cn

Hierarchical control for parallel bidirectional power converters of a grid-connected DC microgrid*

Hui-yong HU†, Yong-gang PENG†‡, Yang-hong XIA, Xiao-ming WANG, Wei WEI, Miao YU

(*College of Electrical Engineering, Zhejiang University, Hangzhou 310027, China*)

†E-mail: huhuiyong@zju.edu.cn; pengyg@zju.edu.cn

Received Aug. 24, 2016; Revision accepted Dec. 29, 2016; Crosschecked Dec. 20, 2017

Abstract: The DC microgrid is connected to the AC utility by parallel bidirectional power converters (BPCs) to import/export large power, whose control directly affects the performance of the grid-connected DC microgrid. Much work has focused on the hierarchical control of the DC, AC, and hybrid microgrids, but little has considered the hierarchical control of multiple parallel BPCs that directly connect the DC microgrid to the AC utility. In this paper, we propose a hierarchical control for parallel BPCs of a grid-connected DC microgrid. To suppress the potential zero-sequence circulating current in the AC side among the parallel BPCs and realize feedback linearization of the voltage control, a *d*-*q*-0 control scheme instead of a conventional *d*-*q* control scheme is proposed in the inner current loop, and the square of the DC voltage is adopted in the inner voltage loop. DC side droop control is applied to realize DC current sharing among multiple BPCs at the primary control level, and this induces DC bus voltage deviation. The quantified relationship between the current sharing error and DC voltage deviation is derived, indicating that there is a trade-off between the DC voltage deviation and current sharing error. To eliminate the current sharing error and DC voltage deviation simultaneously, slope-adjusting and voltage-shifting approaches are adopted at the secondary control level. The proposed tertiary control realizes precise active and reactive power exchange through parallel BPCs for economical operation. The proposed hierarchical control is applied for parallel BPCs of a grid-connected DC microgrid and can operate coordinately with the control for controllable/uncontrollable distributional generation. The effectiveness of the proposed control method is verified by corresponding simulation tests based on Matlab/Simulink, and the performance of the hierarchical control is evaluated for practical applications.

Key words: Parallel bidirectional power converters; Hierarchical control; DC microgrid
https://doi.org/10.1631/FITEE.1601497 **CLC number:** TM91

1 Introduction

With the increasing penetration of renewable energy generation into the modern electric grids, the concept of the microgrid has been proposed for integrating distributed generation and controllable/non-controllable load (Lasseter *et al.*, 2002; Eto *et al.*, 2009). Many types of sources such as photovoltaic (PV) and wind are either inherently DC sources or converted to DC. Loads such as light emitting diode (LED) lighting and DC motors convert AC power to DC before using it. Compared to the AC microgrid, the DC microgrid has a number of advantages due to its high reliability and high efficiency when the distributed generation and load are integrated with the power converters (Xu and Chen, 2011). In the grid-connected mode, the DC microgrid is connected to the AC utility by multiple parallel BPCs to share large exchange power flow (Fig. 1). As the interface between DC microgrid and AC utility, the control of the parallel BPCs directly affects the performance of the grid-connected DC microgrid. Much work has presented the hierarchical control of DC and AC

‡ Corresponding author

* Project supported by the National Natural Science Foundation of China (No. 51377142), the National High-Tech R&D Program (863) of China (No. 2014AA052001), the Zhejiang Provincial Natural Science Foundation of China (No. LY16E070002), and the Zhejiang Province Key R&D Project (No. 2017C01039)

ORCID: Yong-gang PENG, http://orcid.org/0000-0002-0960-3807

microgrids, but little has considered the hierarchical control of multiple parallel BPCs which directly connect the DC microgrid to the AC utility (Bao *et al.*, 2010; Guerrero *et al.*, 2011; Wang *et al.*, 2012; Gao *et al.*, 2013; Lu *et al.*, 2014a; Meng *et al.*, 2015; Torreglosa *et al.*, 2016). Guerrero *et al.* (2011) explained the multilevel hierarchical control according to the standard ISA-95 and introduced the functions of the control levels zero to three of the microgrid. Similarly, the parallel BPCs can be controlled by multiple control levels, which are aimed to make the BPCs operate well and provide power (or voltage) support for the DC microgrid in coordination. We propose a hierarchical control which consists of four levels, including inner control (level 0), primary control (level 1), secondary control (level 2), and tertiary control (level 3), for parallel BPCs of a grid-connected DC microgrid.

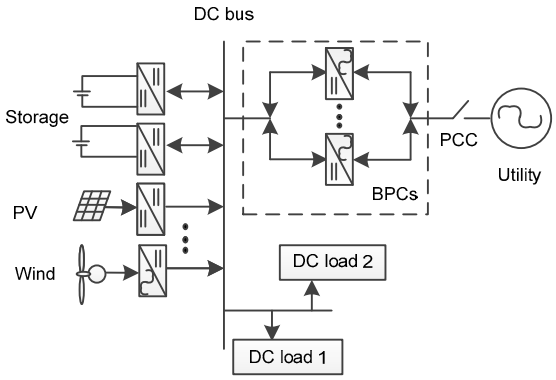

Fig. 1 A typical structure of a grid-connected DC microgrid

At level 0, inner control focuses on suppressing the AC side zero-sequence circulating current and providing DC voltage support for the DC microgrid. When multiple bidirectional power converters are connected input-parallel-output-parallel (Fig. 1), there will be the zero-sequence circulating current between the parallel BPCs. The zero-sequence circulating current decreases the conversion efficiency and increases the power loss of converters. Hence, it is important to reduce the zero-sequence circulating current and achieve accurate power sharing between parallel BPCs (Ye *et al.*, 2002; Pan and Liao, 2008; Zhang *et al.*, 2011; Chen, 2012; Che *et al.*, 2015; Guo *et al.*, 2015; Xiao HG *et al.*, 2016). Ye *et al.* (2002) developed an averaged model of the parallel converters based on a phase-leg averaging technique to predict the dynamics of the zero-sequence circulating current. Pan and Liao (2008) gave a definition of circulating currents for each phase and the corresponding circulating current index, and proposed a coordinate control method of circulating currents for different load conditions. For the grid-connected DC microgrid, the DC bus voltage is supported by the parallel BPCs. A lot of control methods have been proposed for the DC bus voltage (Blasko and Kaura, 1997; Lee, 2003; Bao *et al.*, 2013; Loh *et al.*, 2013). Since the DC voltage of the converters is related to the amplitude of AC current, the control of DC voltage is nonlinear and the whole system is still coupled when the conventional *d-q* axis control scheme is adopted. Lee (2003) adopted an output linearization technology and proposed an outer-loop control strategy to control the square of the DC output voltage, rather than the DC output voltage itself. Bao *et al.* (2013) proposed a simplified feedback linearization (SFL) control strategy for the DC voltage, which can improve the dynamic performance of the DC voltage.

At level 1, the primary control is mainly to realize the DC current sharing among the parallel BPCs and generate the reference voltage for the inner control (Khorsandi *et al.*, 2014; Lu *et al.*, 2014b; Nasirian *et al.*, 2014; 2015; Shafiee *et al.*, 2014; Wang *et al.*, 2016). Lu *et al.* (2014b), Nasirian *et al.* (2014, 2015), and Wang *et al.* (2016) adopted the voltage versus current droop control and proposed an improved distributed secondary control method for DC microgrids. Shafiee *et al.* (2014) set the droop coefficients according to the state-of-charge (SOC) of batteries automatically. Khorsandi *et al.* (2014) adopted the conventional droop control method and estimated line resistances to adjust the droop gains.

At level 2, the secondary control is aimed to eliminate the DC voltage deviation produced by the droop and the current sharing error caused by unequal line impedances. As for coping with the problems, many methods have been presented (Anand *et al.*, 2013; Bidram *et al.*, 2013; Lu *et al.*, 2014a; Nasirian *et al.*, 2014; 2015; Wang *et al.*, 2016). Wang *et al.* (2016) proposed an improved distributed secondary control based on the voltage-shifting and slope-adjusting approaches. The voltage-shifting control is adopted to recover the DC bus voltage, and the slope-adjusting control uses both the average current and

the average droop coefficient to realize equal output impedance. Other distributed controls have also been presented (Anand *et al.*, 2013; Lu *et al.*, 2014a; Nasirian *et al.*, 2014; 2015). Bidram *et al.* (2013) proposed a distributed cooperative control method based on a multi-agent system, and used input-output feedback linearization to convert the secondary voltage control to a linear second-order tracker synchronization problem.

At level 3, the tertiary control mainly regulates the active and reactive exchange power through parallel BPCs. Tertiary control approaches of DC and AC microgrids have been presented (Guerrero *et al.*, 2011; Lu *et al.*, 2014a; Meng *et al.*, 2015; Unamuno and Barrena, 2015; Dragičević *et al.*, 2016; Torreglosa *et al.*, 2016; Xiao HG *et al.*, 2016). Guerrero *et al.* (2011) proposed a general hierarchical control approach toward standardization for droop-controlled AC and DC microgrids. Meng *et al.* (2015) realized the global efficiency optimum based on a genetic algorithm in tertiary control. Xiao JF *et al.* (2016) gave the multilevel energy management control for energy storage, and in tertiary control, autonomous state of charge (SoC) recovery was implemented to limit SoC variation of ES with a high ramp rate. Lu *et al.* (2014a) analyzed four operation modes of hybrid microgrids and their power flow patterns, and gave a hierarchical control of parallel AC-DC converter interfaces for hybrid microgrids for mode (d). The target of tertiary control is to output specific DC current to the external DC grid. Che *et al.* (2015) gave a hierarchical coordination strategy to a community microgrid, which is composed of multiple AC and DC microgrids.

However, this study focuses on a grid-connected DC microgrid, which is connected to the AC utility by parallel bidirectional power converters, and gives a hierarchical control for the parallel BPCs of the grid-connected DC microgrid. To make the BPCs operate well and provide voltage support for the grid-connected DC microgrid in coordination, we propose a hierarchical control for parallel BPCs. First, a 0-axis current control is added to the conventional *d-q* control scheme in the inner current control, and a proportional-integral (PI) controller is applied to make the 0-axis current zero, which suppresses the zero-sequence circulating current. In addition, the square of the DC voltage is adopted in inner voltage control to realize the decoupling control. Second, to obtain equal or proportional import/export power exchange, the DC side decentralized droop control is adopted in primary control. The parallel BPCs can provide voltage support for the grid-connected DC microgrid with DC droop control, but DC side droop control induces DC bus voltage deviation. With the analysis between the current sharing error and DC voltage deviation, there is a trade-off between DC voltage deviation and the current sharing error if only DC droop control is adopted. Third, to avoid the current sharing error caused by unequal line impedances, the slope-adjusting approach is adopted in secondary control to realize equal equivalent output impedance. DC voltage recovery is realized for normal operation of grid-connected microgrid with the voltage-shifting approach in secondary control. Then the current sharing error and DC voltage deviation can be eliminated simultaneously with secondary control. Finally, the precise active and reactive exchange powers through parallel BPCs are realized at the tertiary control level, which improves the schedulable capabilities of the grid-connected microgrid. The proposed hierarchical control can operate coordinately with the control for controllable/uncontrollable distributional generations.

2 System structure of a grid-connected DC microgrid

A typical structure of a grid-connected DC microgrid is shown in Fig. 1. Various types of controllable/uncontrollable distributed generation (DG), such as photovoltaic (PV) and wind generation, are connected to a DC bus through DC/DC or AC/DC converters. The energy storage is connected to a DC bus via bidirectional DC-DC converters to import/export DC power. The DC loads are connected to the DC bus directly or through power electronic interfaces. The DC microgrid is connected to the AC utility by the parallel BPCs to convert DC to AC power, or vice versa, and can operate in the grid-connected mode or island mode by a switch at the point of common coupling (PCC) in the AC side. That is, when the PCC is close, it operates in the grid-connected mode; otherwise, it operates in the island mode. In the grid-connected mode, the uncontrollable

DGs operate in the maximum power point (MPP) to maximize utilization. The controllable (dispatchable) DGs are controlled only by droop control strategies in the grid-connected DC microgrid, and the secondary/tertiary controls for controllable (dispatchable) DGs are disabled in the grid-connected mode. The DC bus voltage is maintained by the parallel BPCs.

When the DC microgrid operates in the grid-connected mode, the large exchanging power flow is shared by the parallel BPCs. Hence, the control for the parallel BPCs is very important.

3 Hierarchical control for the parallel BPCs

In inner control (level 0), the AC side circulating current, which is mainly the zero-sequent current between the parallel BPCs, is suppressed in the inner current control loop by a *d*-*q*-0 control scheme, and the square of the DC voltage is adopted in the inner voltage control loop to realize feedback linearization of voltage control. At the primary control level (level 1), equal or proportional import/export power in the DC side is enhanced by DC voltage-DC current (*V*-*I*) droop control. At the secondary control level (level 2), the DC voltage deviation produced by the droop is eliminated and the current sharing error caused by unequal DC side line impedances is eliminated by voltage-shifting and slope-adjusting approaches. At the tertiary control level (level 3), the precise active exchange power through the parallel BPCs is realized, and the precise reactive exchange power is realized simultaneously. As mentioned above, the uncontrollable DGs in the grid-connected DC microgrid are considered to be operating in the MPP mode in this study. The controllable (dispatchable) DGs are controlled only by droop control strategies in the grid-connected DC microgrid, and the secondary/tertiary controls for controllable (dispatchable) DGs are disabled in the grid-connected mode.

3.1 Inner control (level 0)

The main functions of the inner control are to suppress the AC side zero-sequent circulating current and provide DC bus voltage support for the DC microgrid.

Fig. 2 shows a typical topology of the parallel BPCs system where there are two BPCs. Assume that *k* represents the *k*th BPC. The output AC voltages of the parallel BPCs are $v_{\mathrm{abc},k}$ (k=1, 2) and the voltages of the AC utility are e_{abc}. The output AC currents $i_{\mathrm{abc},k}$ (k=1, 2) are filtered by an inductive filter whose inductance is L_k (k=1, 2) and parasitic resistances are R_k (k=1, 2). s_{abc} (k=1, 2) are the switch functions of converters. The output DC voltages $v_{\mathrm{DC},k}$ (k=1, 2) are filtered by a capacitive filter whose capacitance is C_k (k=1, 2). The line resistances between the capacitive filter and the DC bus are $R_{\mathrm{line},k}$ (k=1, 2). $v_{\mathrm{DC\ bus}}$ is the DC bus voltage of the DC microgrid.

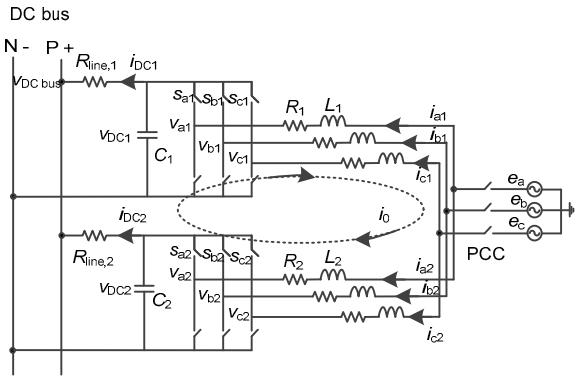

Fig. 2 Topology of the parallel bidirectional power converter system

For a single converter, there is no path for AC zero-sequent current. However, for the input-parallel-output-parallel converters, a zero-sequence current path is formed and a zero-sequence circulating current may occur (Fig. 2) (Ye *et al.*, 2002). To suppress the zero-sequence circulating current, an extra 0-axis control is introduced except for the *d*-*q* axis, which means a *d*-*q*-0 control scheme instead of a conventional *d*-*q* control scheme is adopted.

Because the model of the secondary bidirectional power converter is the same as that of the first bidirectional power converter, the subscripts will be omitted in the following analysis. As shown in Fig. 2, the bidirectional power converter can be modeled as

$$\begin{cases} L\dfrac{\mathrm{d}i_{\mathrm{abc}}}{\mathrm{d}t} = -Ri_{\mathrm{abc}} + e_{\mathrm{abc}} - v_{\mathrm{abc}}, \\ C\dfrac{\mathrm{d}v_{\mathrm{DC}}}{\mathrm{d}t} = s_{\mathrm{abc}}i_{\mathrm{abc}} - i_{\mathrm{DC}}. \end{cases} \tag{1}$$

If S_{a}=1, the upper leg tube in phase a is on and the lower leg tube in phase a is off; if S_{a}=0, the upper leg tube in phase a is off and the lower leg tube in

phase a is on. S_b is for phase b and S_c is for phase c, and they are similar to S_a. v_{DC} is nonlinearly coupled with the AC current i_{abc} and switch functions s_{abc} can be expressed as

$$\begin{bmatrix} x_d \\ x_q \\ x_0 \end{bmatrix} = \frac{2}{3} \begin{bmatrix} \cos\theta & \cos\left(\theta-\frac{2\pi}{3}\right) & \cos\left(\theta+\frac{2\pi}{3}\right) \\ \sin\theta & \sin\left(\theta-\frac{2\pi}{3}\right) & \sin\left(\theta+\frac{2\pi}{3}\right) \\ \frac{1}{2} & \frac{1}{2} & \frac{1}{2} \end{bmatrix} \begin{bmatrix} x_a \\ x_b \\ x_c \end{bmatrix}, \quad (2)$$

where θ is the rotation angle of the reference rotation coordinate system whose angular frequency is ω. $\theta = \int_0^t \omega \mathrm{d}\theta + \theta_0$, and θ_0 is the initial angle. When the d axis is orientated to the grid voltage vector, θ_0=0.

We apply the transformation from a-b-c to d-q-0, which is displayed in Eq. (2) for both sides of Eq. (1). Ignoring the power loss of the switch tubes and parasitic resistance, the instant powers of the AC side and DC side are equal. Reconstructing the model of the system from the energy balance view, the model of the bidirectional power converter in the d-q-0 coordinate system is expressed as

$$\begin{cases} L\dfrac{\mathrm{d}i_d}{\mathrm{d}t} = -Ri_d + \omega L i_q + E_d - v_d, \\ L\dfrac{\mathrm{d}i_q}{\mathrm{d}t} = -Ri_q + \omega L i_d - v_q, \\ L\dfrac{\mathrm{d}i_0}{\mathrm{d}t} = -Ri_0 - v_0, \\ \dfrac{1}{2}C\dfrac{\mathrm{d}v_{DC}^2}{\mathrm{d}t} = \dfrac{3}{2}E_d i_d - P_{DC}, \end{cases} \quad (3)$$

where E_d is the d-axis voltage of the AC utility, P_{DC} is the output DC power of the parallel BPCs in the microgrid, v_d, v_q, and v_0 are the d-, q-, and 0-axis voltages, respectively, and i_d, i_q, and i_0 are the d-, q-, and 0-axis currents, respectively.

From Eq. (3), v_{DC}^2 is linear with i_d regardless of P_{DC}, which is more convenient for control than the nonlinear coupling relationship analyzed above. Furthermore, with the feed forward and decoupling compensation, the active power current i_d and the reactive current i_q can be fully decoupled, which are beneficial for improving the dynamic performance of the system. Based on the model in Eq. (3), the inner control is shown in Fig. 3.

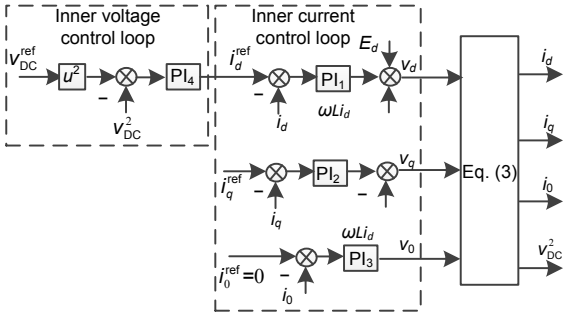

Fig. 3 Inner control loop of the parallel BPCs

i_d^{ref}, i_q^{ref}, and i_0^{ref} are the d-, q-, and 0-axis reference currents, respectively. From the control block diagram in Fig. 3, a d-q-0 control scheme is adopted in the inner current control loop and a v_{DC}^2 feedback control scheme is adopted in the inner voltage control loop. With the 0-axis current control loop, the circulating current among the parallel BPCs can be suppressed. With the v_{DC}^2 feedback and compensation, the whole inner control becomes linear and decoupled, which can improve the performance of the whole inner control.

3.2 Primary control (level 1)

The primary control is mainly to realize DC current sharing and generate the reference voltage for the inner control. If there are some resistance output impedance differences among the parallel BPCs, this will circulate a DC current among the parallel BPCs. To decrease the DC circulating current, DC droop control is applied to obtain equal or proportional import/export power in the primary control. For each BPC, the DC droop control can be expressed as

$$v_{DC,k}^{ref} = v_{DC}^* - r_k(i_{DC,k} - I_{DC,k}^*), \quad (4)$$

where $v_{DC,k}^{ref}$ is the reference voltage for inner control, v_{DC}^* is the rated DC bus voltage, $I_{DC,k}^*$ is the rated output DC current, $i_{DC,k}$ is the actual output DC current, and r_k is the droop coefficient. The DC droop control is shown in Fig. 4.

As shown in Fig. 4, the droop coefficient r_k can be chosen as $(v_{DC}^{max}-v_{DC}^{min})/(I_{DC}^{max}-I_{DC}^{min})$, where v_{DC}^{max} and I_{DC}^{max} are the maximum allowable voltage and output current, respectively, and v_{DC}^{min} and I_{DC}^{min} are the minimum allowable voltage and output current, respectively. To avoid too high or too low voltage, which would be harmful to the DC microgrid, $v_{DC,k}^{ref}$ is set between v_{DC}^{max} and v_{DC}^{min}.

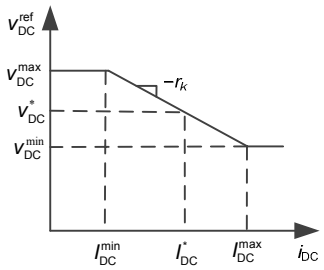

Fig. 4 The DC droop control in the primary control

With the DC droop control applied to each bi-directional power converter, the equivalent circuit of the system with two parallel BPCs is shown in Fig. 5.

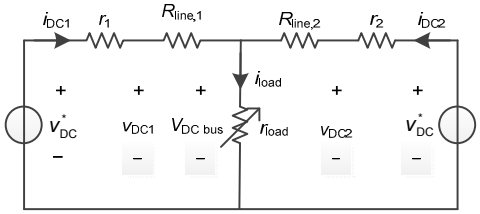

Fig. 5 The equivalent circuit of the parallel BPCs with DC droop control

In Fig. 5, r_{load} is the load resistance and i_{load} is the load current. It can be seen that

$$v_{DC}^{*}-v_{DC\ bus}=i_{DC1}(r_1+R_{line,1})=i_{DC2}(r_2+R_{line,2}). \quad (5)$$

Then, i_{DC1} and i_{DC2} satisfy

$$\frac{i_{DC1}}{i_{DC2}}=\frac{r_2+R_{line,2}}{r_1+R_{line,1}}. \quad (6)$$

In addition, the sum of r_{DC1} and r_{DC2} is equal to r_{load}:

$$i_{DC1}+i_{DC2}=i_{load}. \quad (7)$$

With Eqs. (6) and (7), i_{DC1} and i_{DC2} can be expressed as

$$\begin{cases} i_{DC1}=\dfrac{r_2+R_{line,2}}{r_1+R_{line,1}+r_2+R_{line,2}}i_{load}, \\ i_{DC2}=\dfrac{r_1+R_{line,1}}{r_1+R_{line,1}+r_2+R_{line,2}}i_{load}. \end{cases} \quad (8)$$

Then, the current sharing error Δi_{DC} satisfies

$$\Delta i_{DC}=i_{DC1}-i_{DC2}=\frac{(r_1+R_{line,1})-(r_2+R_{line,2})}{r_1+R_{line,1}+r_2+R_{line,2}}i_{load}. \quad (9)$$

3.3 Secondary control (level 2)

The main function of secondary control is to eliminate the DC voltage deviation and current sharing error. A DC bus voltage deviation is induced when DC droop control is used to achieve DC current sharing among the parallel BPCs.

The relationship between the DC voltage deviation $\Delta v_{DC\ bus}$ and the current sharing error Δi_{DC} can be derived from Eqs. (5), (8), and (9), and is displayed as

$$\begin{aligned}\Delta v_{DC\ bus}&=v_{DC}^{*}-v_{DC\ bus}\\&=\frac{(r_2+R_{line,2})(r_1+R_{line,1})}{(r_1+R_{line,1})-(r_2+R_{line,2})}\Delta i_{DC}.\end{aligned} \quad (10)$$

Generally, current sharing is achieved by large droop coefficients in the primary control, while the DC voltage deviation increases with large droop coefficients according to Eq. (5). So, there is a trade-off between the DC voltage deviation $\Delta v_{DC\ bus}$ and the current sharing error Δi_{DC}. Further, from Eq. (9), the current sharing error Δi_{DC}, which is caused by unequal line impedances, will increase when i_{load} becomes large. Furthermore, if $r_1+R_{line,1}=r_2+R_{line,2}$, then $i_{DC1}=i_{DC2}$, where $R_{line,1}$ and $R_{line,2}$ are the line resistances between the parallel BPCs and the DC bus. To achieve a trade-off between DC voltage deviation $\Delta v_{DC\ bus}$ and current sharing error Δi_{DC}, we eliminate the DC voltage deviation using a voltage-shifting approach and improve the current sharing accuracy using slope-adjusting approaches.

A voltage controller and an average current controller are adopted in secondary control to restore the DC bus voltage and enhance the current sharing accuracy simultaneously. The DC bus voltage and

average value of current are calculated to compare with the DC bus voltage reference and output current of each bidirectional power converter. Proportional-integral (PI) controllers are employed and the output of the PI controllers is added to the droop controller. With the supplement of secondary control, droop control in Eq. (4) can be expanded as Eqs. (11)–(14), and the equivalent output impedance of the kth BPC can be expressed as

$$\delta v_{\mathrm{DC}} = (k_{\mathrm{pv}} + k_{\mathrm{iv}}/s)(v_{\mathrm{DC}}^{*} - v_{\mathrm{DC,\,bus}}), \quad (11)$$

$$\delta r_k = (k_{\mathrm{pi}} + k_{\mathrm{ii}}/s)(i_{\mathrm{DC},\,k} - \sum_{k=1}^{n} i_{\mathrm{DC},\,k}/n), \quad (12)$$

$$v_{\mathrm{DC},k}^{\mathrm{ref}} = v_{\mathrm{DC}}^{*} + \delta v_{\mathrm{DC}} - (r_k - \delta r_k)(i_{\mathrm{DC},k} - I_{\mathrm{DC},k}^{*}), \quad (13)$$

$$r_{\mathrm{equivalent},k} = r_k - \delta r_k + R_{\mathrm{line},k}, \quad (14)$$

where k_{pv} and k_{iv} are the proportional and integral coefficients of the voltage-shifting controller, respectively, and k_{pi} and k_{ii} are the proportional and integral coefficients of the slope-adjusting controller, respectively, v_{DC}^{*} is the reference value of the DC bus voltage, δv_{DC} is the voltage compensation, δr_k is the droop coefficient compensation, and $r_{\mathrm{equivalent},k}$ is the equivalent output impedance of the kth BPC, which is the sum of the total droop coefficient and the actual line impendence.

The voltage compensation to restore the DC bus voltage is the same for each BPC in Eq. (11), and when the equivalent output impedance becomes equal after the slope-adjustment of the droop coefficient, the current sharing accuracy can be ensured.

3.4 Tertiary control (level 3)

The main function of tertiary control is to achieve precise active/reactive power exchange through the parallel BPCs between the DC microgrid and the AC utility. Once the DC microgrid is connected to the AC utility, the power flow can be controlled to realize economical operation.

It can been seen in the tertiary control block diagram (Fig. 6) that the active/reactive power measured at the point of common coupling (PCC) is compared with the specified active/reactive (PQ) reference values P_{g}^{*} and Q_{g}^{*}, which are obtained based on the power requirements of the market situation, i.e., energy cost, storage forecasting, etc. The control laws $\mathrm{PI_P}$ and $\mathrm{PI_Q}$ shown in Fig. 6 can be expressed as

$$\delta v_{\mathrm{DC}}^{*} = k_{\mathrm{pP}}(P_{\mathrm{g}}^{*} - P_{\mathrm{g}}) + k_{\mathrm{iP}}\int (P_{\mathrm{g}}^{*} - P_{\mathrm{g}})\,\mathrm{d}t, \quad (15)$$

$$i_q^{\mathrm{ref}} = k_{\mathrm{pQ}}(Q_{\mathrm{g}}^{*} - Q_{\mathrm{g}}) + k_{\mathrm{iQ}}\int (Q_{\mathrm{g}}^{*} - Q_{\mathrm{g}})\,\mathrm{d}t, \quad (16)$$

where $\delta v_{\mathrm{DC}}^{*}$ is the voltage compensation added to the rated DC bus voltage v_{DC}^{*}, which is the reference value in primary and secondary control, and i_q^{ref} is the q-axis reference current in primary control.

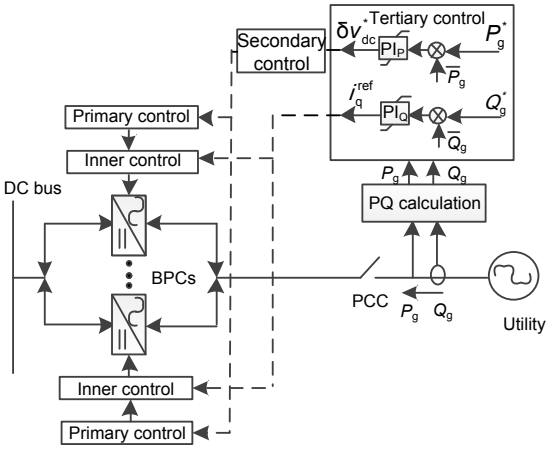

Fig. 6 The tertiary control block diagram of the parallel BPCs

With tertiary control, the reference values in primary and secondary control are improved from v_{DC}^{*} to $v_{\mathrm{DC}}^{*} + \delta v_{\mathrm{DC}}^{*}$. Then, the whole droop control can be expressed as

$$v_{\mathrm{DC},k}^{\mathrm{ref}} = \underbrace{v_{\mathrm{DC}}^{*} - (i_{\mathrm{DC},k} - I_{\mathrm{DC},k}^{*})(r_k}_{\text{Primary}} \underbrace{-\delta r_k) + \delta v_{\mathrm{DC}}}_{\text{Secondary}} \underbrace{+\delta v_{\mathrm{DC}}^{*}}_{\text{Tertiary}}. \quad (17)$$

With active/reactive power regulation in tertiary control, there will be a slight DC bus voltage shift $\delta v_{\mathrm{DC}}^{*}$ when the DC microgrid is operated in grid-connected mode; as a result, $\delta v_{\mathrm{DC}}^{*}$ should be saturated in case it is outside the allowed limits. i_q^{ref} should also be saturated for safe operation.

The proposed tertiary control in the hierarchical control for parallel BPCs does not affect the operation

and power injection of uncontrollable DGs, but affects the controllable DGs through the droop control of controllable DG.

The droop control for the controllable DG can be expressed as

$$v_{\mathrm{DG}}^{\mathrm{ref}} = v_{\mathrm{DG}}^{*} + m_{\mathrm{DG}}(P_{\mathrm{DG0}} - P_{\mathrm{DG}}), \tag{18}$$

where $v_{\mathrm{DG}}^{\mathrm{ref}}$ is the reference voltage for inner control, v_{DG}^{*} is the rated voltage of t, m_{DG} is the droop coefficient, P_{DG0} is the rated power, and P_{DG} is the output power of controllable DG.

From Eq. (18), P_{DG} can be derived as

$$P_{\mathrm{DG}} = P_{\mathrm{DG0}} + (v_{\mathrm{DG}}^{*} - v_{\mathrm{DG}}^{\mathrm{ref}})/m_{\mathrm{DG}}. \tag{19}$$

Since PI controllers are employed in the inner voltage control of both controllable DG and BPCs, in the steady state, $v_{\mathrm{DG}}^{\mathrm{ref}}$ can be expressed as

$$v_{\mathrm{DG}}^{\mathrm{ref}} = v_{\mathrm{DC\ bus}} = v_{\mathrm{DC}}^{*} + \delta v_{\mathrm{DC}}^{*}. \tag{20}$$

Then, P_{DG} can be expressed as

$$P_{\mathrm{DG}} = P_{\mathrm{DG0}} + (v_{\mathrm{DG}}^{*} - v_{\mathrm{DC}}^{*} - \delta v_{\mathrm{DC}}^{*})/m_{\mathrm{DG}}. \tag{21}$$

Substituting $\delta v_{\mathrm{DC}}^{*}$ from Eq. (15), we can obtain

$$P_{\mathrm{DG}} = P_{\mathrm{DG0}} + \frac{v_{\mathrm{DG}}^{*} - v_{\mathrm{DC}}^{*} - k_{\mathrm{pP}}(P_{\mathrm{g}}^{*} - P_{\mathrm{g}}) - k_{\mathrm{iP}}\int (P_{\mathrm{g}}^{*} - P_{\mathrm{g}})\,\mathrm{d}t}{m_{\mathrm{DG}}}. \tag{22}$$

The relationship between the proposed hierarchical control for parallel BPCs and the existing control for controllable DGs is shown in Eq. (22). When the active reference value P_{g}^{*} increases, P_{DG} will reduce, and P_{g} will increase. Eventually, the system achieves a new equilibrium point until $P_{\mathrm{g}}^{*} = P_{\mathrm{g}}$. So, if the proposed tertiary control is active and power import from the utility grid is increased, the output power of the controllable DGs will reduce, while the output power of the uncontrollable DGs remains unchanged.

4 Simulation results and discussion

To verify the effectiveness of the proposed hierarchical control method, a grid-connected DC microgrid of two BPCs (Fig. 7) has been studied. The simulation is conducted in Matlab/Simulink.

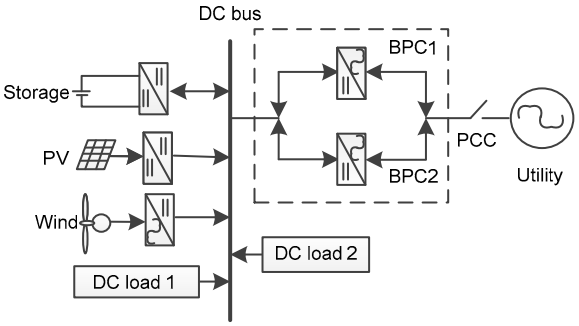

Fig. 7 The study system

The rated AC bus voltage is 311 V and the rated frequency is 50 Hz. R_1=R_2=1 mΩ , L_1=L_2=2 mL, and v_{DC}^{*} =600 V. $R_{\mathrm{line,1}}$=0.06 Ω, $R_{\mathrm{line,2}}$=0.04 Ω, and C_1=C_2=2 mF. The current sharing BPC1:BPC2=1:1. $R_{\mathrm{load,1}}$=5 Ω and $R_{\mathrm{load,2}}$=7.2 Ω. The powers of the PV and wind generation are both 900 kW. $v_{\mathrm{DG}}^{\mathrm{ref}}$=600 V, P_{DG0}=0 kW, and m_{DG}=10 V/100 kW.

In inner control, the controller parameters for BPC1 and BPC2 are the same: PI_1:k_{p1}=4, k_{i1}=100, PI_2:k_{p2}=4, k_{i2}=100, PI_3:k_{p3}=4, k_{i3}=100, PI_4:k_{p4}=0.001, and k_{i4}=0.1. In primary control, $I_{\mathrm{DC,1}}^{*} = I_{\mathrm{DC,2}}^{*} = 0$, r_1=r_2=0.04. In secondary control, k_{pv}=1, k_{iv}=200, k_{pi}=0.001, k_{ii}=0.01. In tertiary control, $\mathrm{PI_P}$:k_{pP}=0.0005, k_{iP}=0.001, $\mathrm{PI_Q}$:k_{pQ}=0.005, and k_{iQ}=0.03.

The grid-connected microgrid is started with DC load 1, wind generation, and energy storage. The DC bus voltage is supported by the parallel BPCs, which convert the energy between the grid-connected microgrid and the AC utility. Load 2 is connected to the DC bus at 2.5 s, and the PV generation, which outputs 90 kW, is connected to the DC bus at 4.5 s. The secondary control is activated at 6.5 s for DC bus voltage recovery and DC current sharing, and the tertiary control is activated at 8.5 s for controlling the exchange power at PCC. The active power reference value is −60 kW and has a step to −30 kW at 10 s. The reactive power reference value is 10 kV·A and has a step to −10 kV·A at 10 s.

Fig. 8 shows the AC current of the BPCs in phase b: conventional *d*-*q* axis control in Fig. 8a, and proposed *d*-*q*-0 axis control in Fig. 8b. The sum of BPC1 and BPC2 current in Figs. 8a and 8b are both smooth, which means that there are no asymmetrical components in the sum current. The currents of BPC1 and BPC2 in Fig. 8a are both fluctuant, indicating that there is a circulating current between BPC1 and BPC2. In contrast, the BPC1 and BPC2 currents in Fig. 8b are smooth, indicating that the circulating current has been suppressed by the 0-axis control.

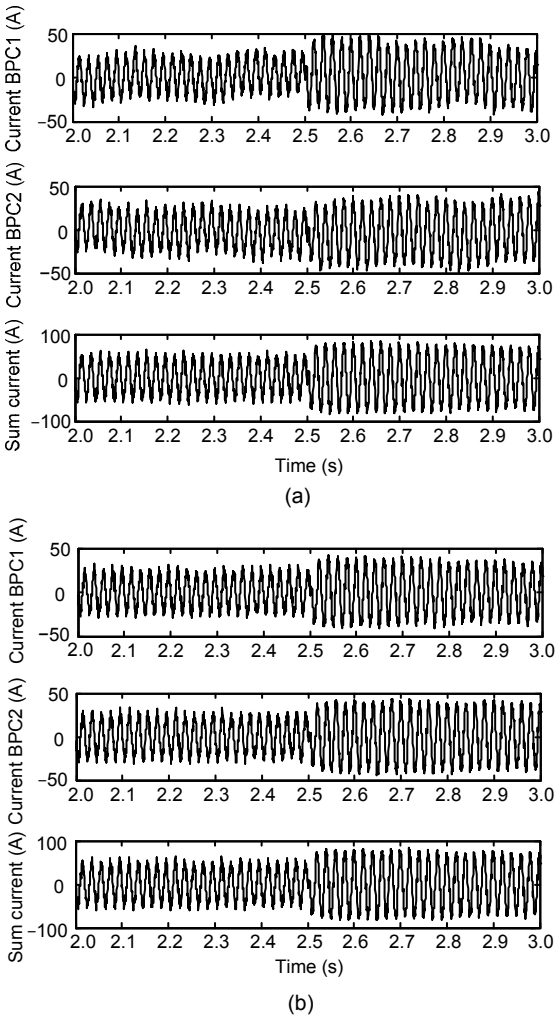

Fig. 8 The AC current of BPCs in phase b: (a) conventional *d*-*q* axis control; (b) proposed *d*-*q*-0 axis control

Fig. 9 shows the performance of the primary and secondary control. Fig. 9a shows the changes of DC bus voltage. Before the secondary control is activated, the DC bus voltage is controlled within 590–610 V as steady by the DC droop control, and can be recovered immediately to the rated voltage 600 V with the secondary control. Fig. 9b shows the changes of actual output DC current of BPC1 and BPC2. With the output power of PV generation at 4.5 s, the power of the sources is larger than the load. Then, the DC current of the parallel BPCs is reversed to output power to the AC utility. Before the secondary control is activated, r_1=r_2=0.04 Ω, but the line impendences of BPC1 and BPC2 are 0.06 Ω and 0.04 Ω, respectively. The performance of the droop control is affected by the mismatch impedance of parallel BPCs, and the current sharing error increases when the output current increases. Before 4.5 s, the steady error of i_{DC1} and i_{DC2} is about 4 A, but it increases to about

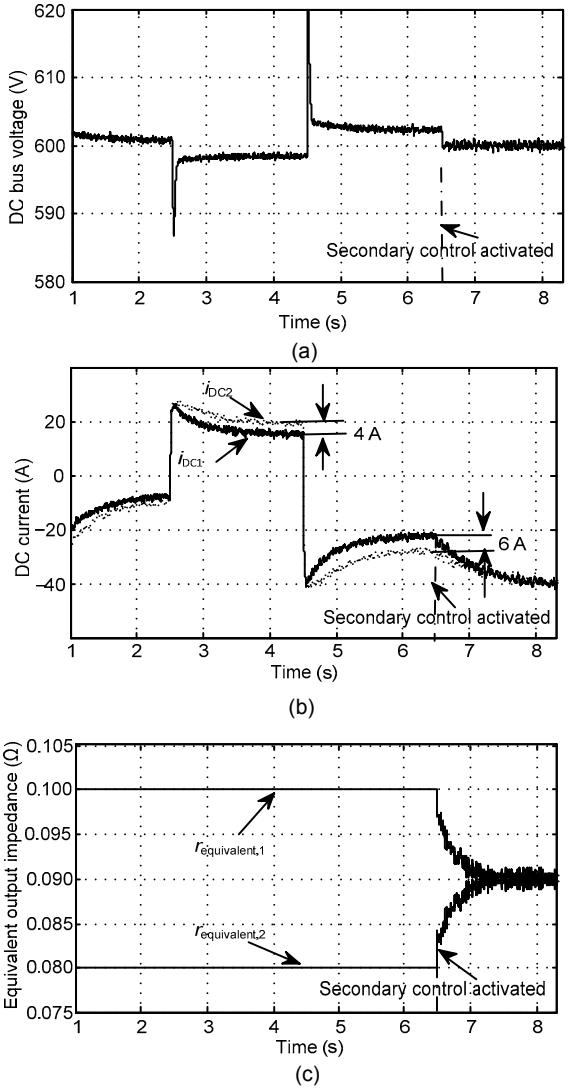

Fig. 9 The performance of primary and secondary control: (a) DC bus voltage; (b) DC currents of BPCs; (c) equivalent output impedances of BPCs

6 A after 4.5 s. Fig. 9c shows the equivalent output impedances of the BPCs. Before the secondary control is activated, the equivalent output impedances of BPC1 and BPC2 are 0.1 Ω and 0.08 Ω, respectively, and equal to 0.09 Ω with the adjustment of secondary control, which improves the current sharing accuracy of i_{DC1} and i_{DC2} after 6.5 s (Fig. 9b).

The performance of tertiary control is shown in Fig. 10. The active/reactive power reference value has a step at 10 s, which means that the actual active/reactive exchange power at PCC follows the active/reactive power reference value as expected.

The output powers of wind/PV/storage are shown in Fig. 11. The output powers of wind/PV, which are uncontrollable DGs, are unchanged when the active/reactive power reference value increases at 10 s, while the output power of storage, which is a controllable DG, reduces when the active/reactive power reference value increases at 10 s. The results confirm the theoretical analysis in Section 3.4.

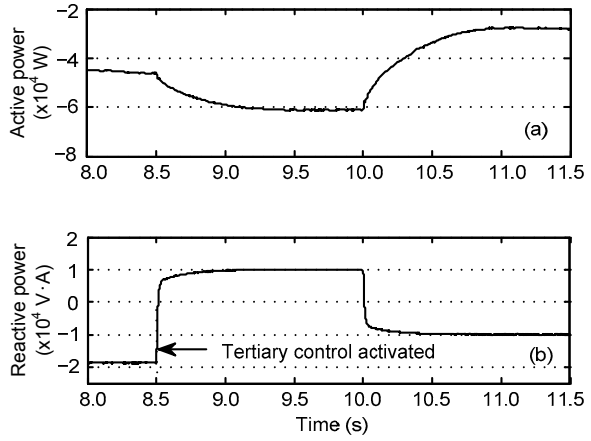

Fig. 10 The performance of tertiary control: (a) active power; (b) reactive power

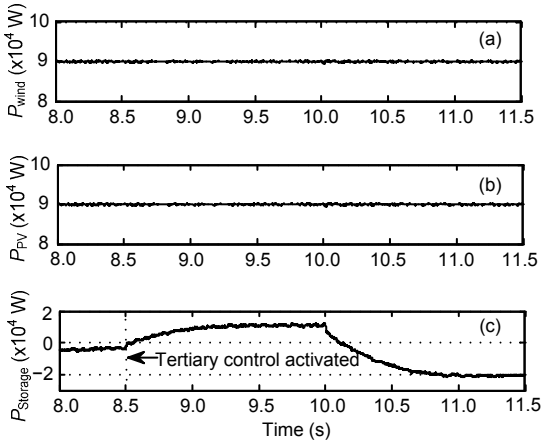

Fig. 11 The output power of DGs: (a) power of wind; (b) power of PV; (C) power of storage

5 Conclusions

A hierarchical control for parallel bidirectional power converters of a grid-connected DC microgrid is proposed. The potential AC-side zero-sequence circulating current between parallel BPCs is suppressed by the proposed *d*-*q*-0 control scheme. The quantified relationship between the current sharing error and DC voltage deviation is derived, indicating that there is a trade-off between the DC voltage deviation and the current sharing error. With the slope-adjusting and voltage-shifting approaches at the secondary control level, the current sharing error and DC voltage deviation are eliminated simultaneously. The precise active and reactive power exchange through parallel BPCs for economical operation are realized with the proposed tertiary control. The proposed hierarchical control for parallel BPCs can operate coordinately with the control for controllable/uncontrollable distributional generation. The effectiveness of the proposed hierarchical control is verified by corresponding simulation tests based on Matlab/Simulink, and the performance of hierarchical control is evaluated for practical applications.

The proposed hierarchical control method for parallel BPCs can effectively share the large exchange power flow and provide voltage support for the grid-connected microgrid. Moreover, the schedulable capability of the grid-connected microgrid is improved for economical operation.

References

Anand, S., Fernandes, B.G., Guerrero, J., 2013. Distributed control to ensure proportional load sharing and improve voltage regulation in low-voltage DC microgrids. *IEEE Trans. Power Electron.*, **28**(4):1900-1913. https://doi.org/10.1109/TPEL.2012.2215055

Bao, J.Y., Bao, W.B., Zhang, Z.C., 2010. Generalized multilevel current source inverter topology with self-balancing current. *J. Zhejiang Univ.-Sci. C (Comput. & Electron.)*, **11**(7):555-561. https://doi.org/10.1631/jzus.C0910605

Bao, X.W., Zhuo, F., Tian, Y., *et al*., 2013. Simplified feedback linearization control of three-phase photovoltaic inverter with an LCL filter. *IEEE Trans. Power Electron.*, **28**(6):

2739-2752.
https://doi.org/10.1109/TPEL.2012.2225076

Bidram, A., Davoudi, A., Lewis, F.L., *et al*., 2013. Distributed cooperative secondary control of microgrids using feedback linearization. *IEEE Trans*. *Power Syst*., **28**(3):3462-3470. https://doi.org/10.1109/TPWRS.2013.2247071

Blasko, V., Kaura, V., 1997. A novel control to actively damp resonance in input LC filter of a three-phase voltage source converter. *IEEE Trans*. *Ind*. *Appl*., **33**(2):542-550. https://doi.org/10.1109/28.568021

Che, L., Shahidehpour, M., Alabdulwahab, A., *et al*., 2015. Hierarchical coordination of a community microgrid with AC and DC microgrids. *IEEE Trans*. *Smart Grid*, **6**(6):3042-3051. https://doi.org/10.1109/TSG.2015.2398853

Chen, T.P., 2012. Zero-sequence circulating current reduction method for parallel HEPWM inverters between AC bus and DC bus. *IEEE Trans*. *Ind*. *Electron*., **59**(1):290-300. https://doi.org/10.1109/TIE.2011.2106102

Dragičević, T., Lu, X.N., Vasquez, J.C., *et al*., 2016. DC microgrids-part I: A review of control strategies and stabilization techniques. *IEEE Trans*. *Power Electron*., **31**(7):4876-4891. https://doi.org/10.1109/TPEL.2015.2478859

Eto, J., Lasseter, R., Schenkman, B., *et al*., 2009. Overview of the CERTS microgrid laboratory test bed. *IEEE Trans. Power Del.*, **26**(1):325-332. https://doi.org/10.1109/TPWRD.2010.2051819

Gao, M.Z., Chen, M., Jin, C., *et al*., 2013. Analysis, design, and experimental evaluation of power calculation in digital droop-controlled parallel microgrid inverters. *J. Zhejiang Univ.-Sci. C (Comput. & Electron.)*, **14**(1):50-64. https://doi.org/10.1631/jzus.C1200236

Guerrero, J.M., Vasquez, J.C., Matas, J., *et al*., 2011. Hierarchical control of droop-controlled AC and DC microgrids—a general approach toward standardization. *IEEE Trans*. *Ind*. *Electron*., **58**(1):158-172. https://doi.org/10.1109/TIE.2010.2066534

Guo, T.T., Liu, X.L., Hao, S.Q., *et al*., 2015. Analysis and design of pulse frequency modulation dielectric barrier discharge for low power applications. *Front*. *Inform*. *Technol*. *Electron*. *Eng*., **16**(3):249-258. https://doi.org/10.1631/FITEE.1400185

Khorsandi, A., Ashourloo, M., Mokhtari, H., 2014. A decentralized control method for a low-voltage DC microgrid. *IEEE Trans*. *Energy Conv*., **29**(4):793-801. https://doi.org/10.1109/TEC.2014.2329236

Lasseter, R., Akhil, A., Marnay, C., *et al*., 2002. Consortium for Electric Reliability Technology Solutions. White Paper on Integration of Distributed Energy Resources. The CERTS MicroGrid Concept, p.1-29.

Lee, T.S., 2003. Input-output linearization and zero-dynamics control of three-phase AC/DC voltage-source converters. *IEEE Trans*. *Power Electron*., **18**(1):11-22. https://doi.org/10.1109/TPEL.2002.807145

Loh, P.C., Li, D., Chai, Y.K., *et al*., 2013. Autonomous control of interlinking converter with energy storage in hybrid AC-DC microgrid. *IEEE Trans*. *Ind*. *Appl*., **49**(3):1374-1382. https://doi.org/10.1109/TIA.2013.2252319

Lu, X.N., Guerrero, J.M., Sun, K., *et al*., 2014a. Hierarchical control of parallel AC-DC converter interfaces for hybrid microgrids. *IEEE Trans*. *Smart Grid*, **5**(2):683-692. https://doi.org/10.1109/TSG.2013.2272327

Lu, X.N., Guerrero, J.M., Sun, K., *et al*., 2014b. An improved droop control method for DC microgrids based on low bandwidth communication with DC bus voltage restoration and enhanced current sharing accuracy. *IEEE Trans*. *Power Electron*., **29**(4):1800-1812. https://doi.org/10.1109/TPEL.2013.2266419

Meng, L.X., Dragicevic, T., Vasquez, J.C., *et al*., 2015. Tertiary and secondary control levels for efficiency optimization and system damping in droop controlled DC-DC converters. *IEEE Trans*. *Smart Grid*, **6**(6):2615-2626 https://doi.org/10.1109/TSG.2015.2435055

Nasirian, V., Davoudi, A., Lewis, F.L., *et al*., 2014. Distributed adaptive droop control for DC distribution systems. *IEEE Trans*. *Energy Conv*., **29**(4):944-956. https://doi.org/10.1109/TEC.2014.2350458

Nasirian, V., Moayedi, S., Davoudi, A., *et al*., 2015. Distributed cooperative control of DC microgrids. *IEEE Trans*. *Power Electron*., **30**(4):2288-2303. https://doi.org/10.1109/TPEL.2014.2324579

Pan, C.T., Liao, Y.H., 2008. Modeling and control of circulating currents for parallel three-phase boost rectifiers with different load sharing. *IEEE Trans*. *Ind*. *Electron*., **55**(7):2776-2785. https://doi.org/10.1109/TIE.2008.925647

Shafiee, Q., Dragičević, T., Vasquez, J.C., *et al*., 2014. Hierarchical control for multiple DC-microgrids clusters. *IEEE Trans*. *Energy Conv*., **29**(4):922-933. https://doi.org/10.1109/TEC.2014.2362191

Torreglosa, J.P., García-Triviño, P., Fernández-Ramirez, L.M., *et al*., 2016. Control strategies for DC networks: a systematic literature review. *Renew*. *Sust*. *Energy Rev*., **58**:319-330. https://doi.org/10.1016/j.rser.2015.12.314

Unamuno, E., Barrena, J.A., 2015. Hybrid ac/dc microgrids—Part II: review and classification of control strategies. *Renew*. *Sustain*. *Energy Rev*., **52**:1123-1134. https://doi.org/10.1016/j.rser.2015.07.186

Wang, L.J., Yang, T., Zhang, D.M., *et al*., 2012. A high performance simulation methodology for multilevel grid-connected inverters. *J. Zhejiang Univ.-Sci. C (Comput. & Electron.)*, **13**(7):544-551. https://doi.org/10.1631/jzus.C1100315

Wang, P.B., Lu, X.N., Yang, X., *et al*., 2016. An improved distributed secondary control method for DC microgrids with enhanced dynamic current sharing performance. *IEEE Trans*. *Power Electron*., **31**(9):6658-6673. https://doi.org/10.1109/TPEL.2015.2499310

Xiao, H.G., Luo, A., Shuai, Z.K., *et al*., 2016. An improved control method for multiple bidirectional power convert-

ers in hybrid AC/DC microgrid. *IEEE Trans*. *Smart Grid*, **7**(1):340-347. https://doi.org/10.1109/TSG.2015.2469758

Xiao, J.F., Wang, P., Setyawan, L., 2016. Multilevel energy management system for hybridization of energy storages in DC microgrids. *IEEE Trans*. *Smart Grid*, **7**(2):847-856. https://doi.org/10.1109/TSG.2015.2424983

Xu, L., Chen, D., 2011. Control and operation of a DC microgrid with variable generation and energy storage. *IEEE Trans*. *Power Del*., **26**(4):2513-2522. https://doi.org/10.1109/TPWRD.2011.2158456

Ye, Z.H., Boroyevich, D., Choi, J.Y., *et al*., 2002. Control of circulating current in two parallel three-phase boost rectifiers. *IEEE Trans*. *Power Electron*., **17**(5):609-615. https://doi.org/10.1109/TPEL.2002.802170

Zhang, D., Wang, F.F., Burgos, R., *et al*., 2011. Common-mode circulating current control of paralleled interleaved three-phase two-level voltage-source converters with discontinuous space-vector modulation. *IEEE Trans*. *Power Electron*., **26**(12):3925-3935. https://doi.org/10.1109/TPEL.2011.2131681